



CHORUS

This is the accepted manuscript made available via CHORUS. The article has been published as:

Length Scale of the Spin Seebeck Effect

Andreas Kehlberger, Ulrike Ritzmann, Denise Hinzke, Er-Jia Guo, Joel Cramer, Gerhard Jakob, Mehmet C. Onbasli, Dong Hun Kim, Caroline A. Ross, Matthias B. Jungfleisch, Burkard Hillebrands, Ulrich Nowak, and Mathias Kläui

Phys. Rev. Lett. **115**, 096602 — Published 28 August 2015

DOI: [10.1103/PhysRevLett.115.096602](https://doi.org/10.1103/PhysRevLett.115.096602)

Length scale of the spin Seebeck effect

Andreas Kehlberger,^{1,*} Ulrike Ritzmann,² Denise Hinzke,² Er-Jia Guo,¹ Joel Cramer,¹ Gerhard Jakob,¹ Mehmet C. Onbasli,³ Dong Hun Kim,³ Caroline A. Ross,³ Matthias B. Jungfleisch,⁴ Burkard Hillebrands,⁴ Ulrich Nowak,² and Mathias Kläui^{1,*}

¹*Institute of Physics, Johannes Gutenberg-University Mainz, 55099 Mainz, Germany*

²*Department of Physics, University of Konstanz, D-78457 Konstanz, Germany*

³*Department of Materials Science and Engineering,*

Massachusetts Institute of Technology, Cambridge, Massachusetts 02139, USA

⁴*Fachbereich Physik and Landesforschungszentrum OPTIMAS,*

Technische Universität Kaiserslautern, Kaiserslautern 67663, Germany

(Dated: August 6, 2015)

We investigate the origin of the spin Seebeck effect in Yttrium Iron Garnet (YIG) samples for film thicknesses from 20 nm to 50 μm at room temperature and 50 K. Our results reveal a characteristic increase of the longitudinal spin Seebeck effect (LSSE) amplitude with the thickness of the insulating ferrimagnetic YIG, which levels off at a critical thickness that increases with decreasing temperature. The observed behavior cannot be explained as an interface effect or by variations of the material parameters. Comparison to numerical simulations of thermal magnonic spin currents yields qualitative agreement for the thickness dependence resulting from the finite magnon propagation length. This allows us to trace the origin of the observed signals to genuine bulk magnonic spin currents due to the spin Seebeck effect ruling out an interface origin and allowing us to gauge the reach of thermally excited magnons in this system for different temperatures. At low temperature even quantitative agreement with the simulations is found.

PACS numbers: 72.20.Pa, 72.25.-b, 75.30.Ds, 75.40.Gb

The thermal excitation of a spin current by a temperature gradient is commonly called the spin Seebeck effect (SSE) which is detected by the inverse spin Hall effect (ISHE) [1, 2], leading to a thermo-voltage similar to the charge analogue, the Seebeck effect. Experimental evidence of the SSE first in ferromagnetic metals [3] and, later, both in semiconductors [4] and in insulators [5–8] has brought up the question about the origin of the SSE. Of particular interest for spin-caloritronics is the observation of the SSE in insulators, which allows to generate pure spin currents in insulating systems.

However, the underlying mechanism, properties, and the origin of the observed signals have been highly controversial. Thermally induced magnonic spin currents have been suggested as the origin [9, 10], based on the presence of the effect in magnetic insulators, which excludes charge currents as the source. Despite this explanation of the origin of the effect, direct experimental evidence has not been reported. While parasitic interface effects [11] were suggested as alternative source of the SSE due to a polarization of the paramagnetic detector layer [12], generally the observed effects are now primarily attributed to magnonic spin currents [13, 14].

Time resolved experiments trying to address the problem by probing the temporal evolution of the SSE have obtained contradicting results: For film thickness up to 61 nm, no cut off frequency due to an intrinsic limitation by the SSE was observed [15]. In contrast, for μm thick films, a characteristic rise time was found, and a finite magnon propagation length of the order of several 100 nm was put forward as a possible explanation [16, 17].

This clearly calls for study to reveal the origin of this discrepancy as it underlies the fundamental mechanism of the SSE and determine the intrinsic length scale.

To clarify the origin of the measured SSE signals, we present a detailed study of the relevant length scales of the longitudinal SSE (LSSE) covering the full range from nm to μm thick $\text{Y}_3\text{Fe}_5\text{O}_{12}$ [18, 19] samples covered by platinum (YIG/Pt). By varying the thickness of the ferrimagnetic insulator and careful control of the interface quality we are able to detect a characteristic feature of the SSE: Our results show an increasing and saturating SSE signal with increasing YIG film thickness. Furthermore we find a temperature dependence for the saturation of the SSE, which shows an increasing intrinsic length scale for the SSE at lower temperatures. Atomistic spin simulation of the propagation of exchange magnons in temperature gradients can qualitatively reproduce the experimentally observed behavior, highlighting that we are able to observe a true magnonic origin of the SSE, revealing its bulk origin even in YIG/Pt.

YIG samples with thicknesses from 20 nm to 50 μm were grown by pulsed laser deposition (PLD) [20, 21] and liquid phase epitaxy (LPE) on $\text{Gd}_3\text{Ga}_5\text{O}_{12}$ substrates [19] and capped with Pt as detailed in the supplementary information [22]. The PLD samples are sorted into series, indicating an identical interface treatment and simultaneous Pt deposition, leading to an identical interface and Pt thickness [23] for all samples within a series. A schematic depiction of the final sample structure is shown in the inset of Fig. 1a).

Magnetometry shows constant magnetic properties for

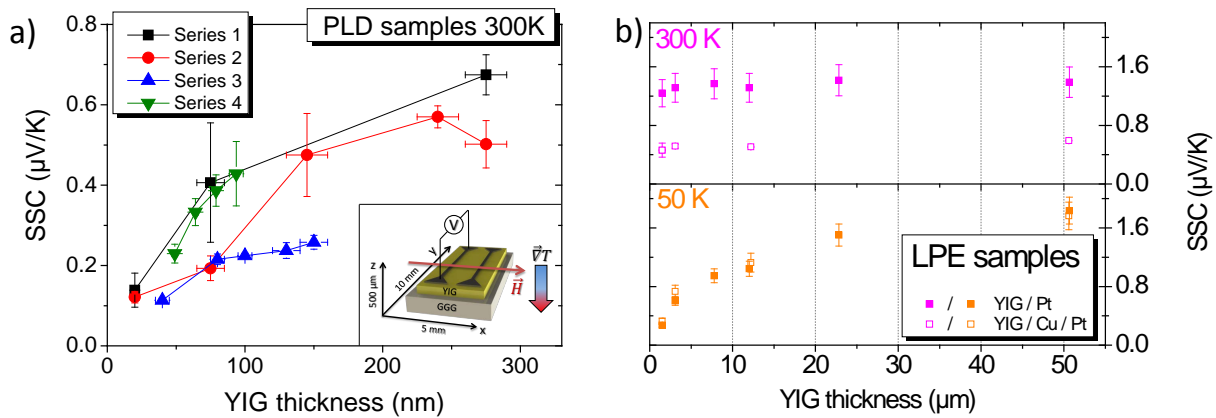


Figure 1. Spin Seebeck coefficient as a function of YIG layer thickness for samples produced by PLD a) and LPE b). The series sorting for the PLD samples highlights an identical interface. Data points are connected for clarity. The inset of a) shows a schematic depiction of the sample structure and setup.

the films, except for the 20 nm films, as shown together with more details on sample fabrication and an analysis of the spin diffusion length of the Pt layer [8, 24] in supplementary information [22], which includes Ref. [25].

The spin Seebeck measurements are performed at room temperature (RT) and in a cryostat at 50 K. Both setups use the LSSE geometry [26], where the temperature gradient is applied out-of-plane. To parametrize the SSE, we make use of the spin Seebeck coefficient (SSC), describing the SSE signal strength per degree of temperature difference applied on the system. A more detailed description of the setups is presented in Ref. [27] and in the supplementary information [22].

First we will discuss our results obtained for the SSC in the PLD grown samples at RT (Fig. 1a)). Films below ~ 90 nm show an increase of the signal amplitude with increasing thickness, in agreement with observations for polycrystalline Bi substituted YIG [28]. For the epitaxial pure YIG films, we find for larger thicknesses a decreasing slope, leading to a saturation of the signal. The samples of series 3 generated signals a factor of two lower than the other series, attributed to the lack of interface etching prior to the Pt deposition, which leads to a less transparent interface for the magnons and, therefore, a smaller spin mixing conductance [29]. This observation underlines the importance of the interface conditions for the comparison of different samples, but the absolute trend of the thickness dependence is not affected.

To exclude an influence of the MR effect in the Pt [30], we perform four point resistance measurements of the Pt-stripe and determine the MR ratio between in-plane \perp and \parallel orientation for samples of series 2 and 3. Similarly to the intrinsic material parameters, the MR ratio shows no systematic dependence on the film thickness, which allows us to conclude that the source of the observed signals is not caused by a proximity magnetization layer at the interface [11] and that the clear thickness depen-

dence points to an origin in the bulk of the YIG. The corresponding measurements are provided in the supplementary information [22].

To show that the observed behavior is a generic property of the SSE and not limited to PLD-grown samples, we next investigate LPE grown YIG, which allows for the growth of high-quality μm thick films, shown in Fig. 1b). While the LPE samples used have a $\{111\}$ surface texture different compared to $\{100\}$ of the PLD samples, we also measured both orientations for the same thicknesses, which yield no noticeable difference for the SSE signals, allowing us to compare both sets of samples. At RT, the SSC is constant for thicknesses above $1.5 \mu\text{m}$, showing that the signal is saturated at those thicknesses. This saturation behavior matches with our expectation obtained from the PLD samples, which suggest the increasing signal with YIG thickness can only be observed for samples thinner than $1 \mu\text{m}$. However, at a temperature of 50 K, we find a thickness dependence qualitatively similar to the PLD samples. The lower graph in Fig. 1b) shows the signal increase with YIG thickness, with a levelling off above a thickness of $20 \mu\text{m}$. To rule out any proximity - induced effects, we measured the thickness dependence in a second series of LPE grown films with a 2 nm thick Cu spacer layer between the YIG and Pt detection layer. This separation layer allows us to exclude any additional influence of a parasitic signal contribution to detected ISHE-voltages. Identical to the LPE samples, having only a Pt detection layer, the SSE signals show no dependency on the YIG thickness at RT, revealing only a within the error constant signal. Compared to the samples without Cu spacing layer, the SSC is reduced due to the high conductivity of the Cu, which shortcuts the electron accumulation in the Pt detection layer [31], leading to a lower ISHE voltage in the samples with a Cu spacer layer. At 50 K the SSE shows the identical behavior as for the samples with only Pt by revealing

an increasing signal for thinner films and leveling off for thicker samples.

To understand this universal behavior of an increasing and saturating signal with increasing film thickness, we assume for our calculations that the influence of the YIG thickness on the SSE might be due to a finite length scale for magnon propagation in the YIG. To investigate this, we simulate the propagation of thermally excited magnons in a temperature gradient using an atomistic spin model which is able to describe the full magnon frequency spectra. Our generic model contains a ferromagnetic nearest-neighbor exchange interaction J and a uniaxial anisotropy with easy-axis along the z -direction and anisotropy constant $d_z = 0.1J$. We investigate a cubic system with $8 \times 8 \times 512$ spins, initialized parallel to the z -axis. The dynamics of the spin system are calculated by solving the stochastic Landau-Lifshitz-Gilbert equation numerically with the Heun-Method [32]. The phonons provide a heat-bath for the spin system assuming a linear temperature gradient (constant during the simulation) over the length L in the z -direction as shown in Fig. 2. Here, for simplicity, we assume that the temperature of the cold area, acting as the contact to the nonmagnetic material, is zero. After an initial relaxation, the local, reduced magnetization $m(z)$ is determined as an average over all spins \mathbf{S}_i in the corresponding x - y -plane and, additionally, as an average over time.

Due to the temperature gradient, magnons propagate from the hotter towards the colder region leading to deviations of the local magnetization $m(z)$ from its local equilibrium value $m_0(z)$, which would follow from the local temperature $T_p(z)$ of the phonon system. A temperature dependent calculation of the equilibrium magnetization $m_0(T)$ for a system with constant temperature allows us to define a magnon accumulation $\Delta m(z) = m(z) - m_0(T_p(z))$ [33].

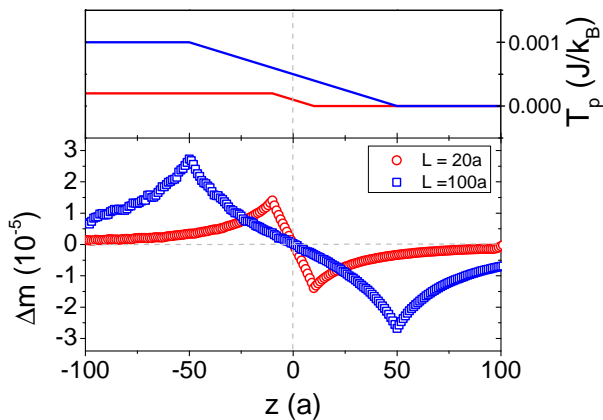


Figure 2. Magnon accumulation Δm as a function of the spatial coordinate z in units of the cubic lattice constant a for a given phonon temperature T_p including a temperature gradient over two different lengths L .

Fig. 2 exemplifies this magnon accumulation Δm as a function of spatial coordinate z in a system with a damping constant of $\alpha = 0.01$ and a linear temperature gradient of $\nabla T = 10^{-5} J / (k_B a)$ over two different lengths L , where a is the lattice constant of the cubic system. At the hotter end of the gradient magnons propagate towards the cooler region, increasing the local magnetization. At the cold end of the gradient, magnons arriving from hotter parts of the system decrease the local magnetization. The resulting magnon accumulation is symmetric in space and changes its sign at the center of the temperature gradient.

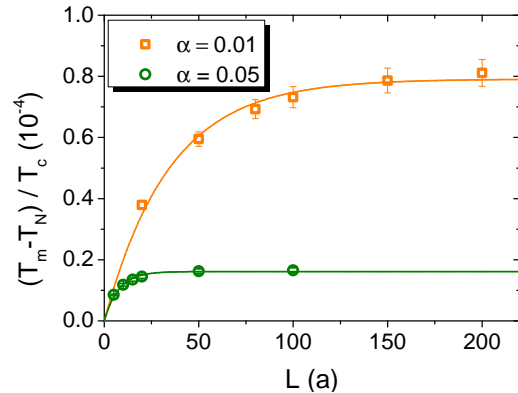


Figure 3. Numerical data of the temperature difference $T_m - T_N$ at the cold end of the temperature gradient in units of the Curie temperature T_c as a function of the length L of the temperature gradient for two different damping constants α . The solid lines corresponds to a fit using eq. 1.

The magnon accumulation at the cold end of the gradient increases with increasing length L . The temperature difference $T_m - T_N$ at the cold end of the gradient can be calculated from the local magnon accumulation. Following Xiao et al. [9] this temperature difference can be related to the magnonic spin current, which is propagating to the detector material and measured in experiments. Fig. 3 shows this temperature difference for two different damping constants. For small length L the temperature difference increases with increasing thickness until a saturation value is reached. The characteristic length scale of the saturation depends on the damping constant. Previously we have shown that the propagation length of the magnons scales with $1/\alpha$ [33]. In a temperature gradient, where a broad distribution of frequencies contributes, the mean value of the propagation length scales similarly, to first order. The magnon spin current can be understood as the averaged sum of magnons, reaching the end of the gradient. As illustrated in Fig. 4 only those magnons from distances smaller than their propagation length contribute to the resulting magnonic spin current at the cold end of the temperature gradient.

Therefore a saturation of the magnonic spin current

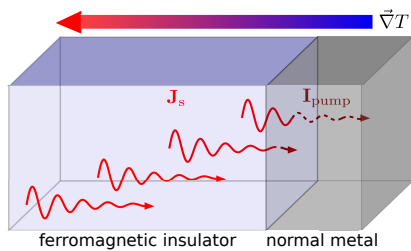


Figure 4. Illustration of a finite magnon propagation length. The net magnon current carries angular momentum antiparallel to the thermal gradient. Only magnons excited at distances smaller than their propagation length contribute to detected signal, leading to a saturation effect.

sets in if the length overcomes the mean propagation length of the magnons. The saturation behavior can be described by

$$T_m - T_N \propto (1 - \exp(-L/\xi)), \quad (1)$$

where ξ describes the mean propagation length of the magnons. A fit of the numerical data is included in Fig. 3 as solid lines and can describe the observed saturation behavior and the dependence on the damping constant.

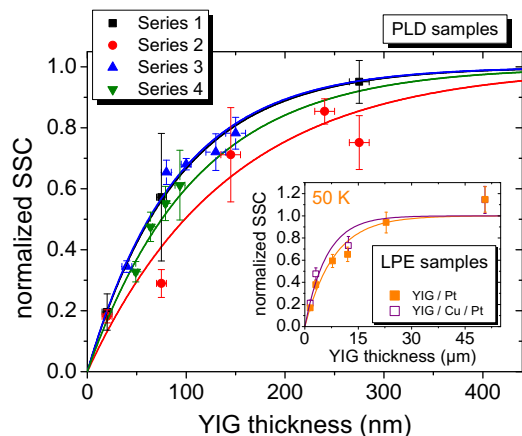


Figure 5. Normalized SSC data and corresponding fit functions plotted as a function of the YIG thickness for PLD and for the LPE sample at 50 K in the inset. The SSC data have been normalized to the saturation value for an infinitely large system. The lines show the fit via eq. 1.

Due to the large computational effort of the performed simulation, it is not possible to simulate the YIG system. To compare the value with the experimental results we extrapolate the numerical data towards lower damping and lower anisotropy. From measurements, we obtain a mean damping constant of $\alpha = 2.5 \times 10^{-4}$ for the LPE films and $\alpha = 4.5 \times 10^{-4}$ for the PLD samples at 300 K [20]. To take into account the temperature dependence of the damping parameter, we use in the

0 K simulations a damping parameter of $\alpha = 1 \times 10^{-4}$. We expect that the dominant anisotropy contribution is given by the shape anisotropy and using the value for the saturation magnetization we estimate an anisotropy constant of about $d_z = 10^{-4} J$. Using a $1/\alpha$ -scaling of the mean propagation length and including the dependence on the frequency gap and therefore on the anisotropy reported by Ritzmann et al. [34] we extrapolate a mean propagation length of about 10 μm from the numerical calculations.

As shown in Fig. 5, we evaluate each series with eq. 1, obtaining mean magnon propagation lengths between 90 nm and 140 nm for the PLD samples, while for the LPE samples at RT we can only give an upper limit for propagation length of 1 μm , in agreement with the time dependent measurements [16, 17]. For 50 K the fit yields a value of $(8 \pm 2) \mu\text{m}$ for the YIG / Pt samples and a comparable one of $(6 \pm 2) \mu\text{m}$ for the samples with a Cu spacing layer. Both values are close to the value of 10 μm estimated from the simulations for 0 K.

We would like to point out, that our result of a finite volume of the YIG contributing to the measured SSE signals allows us to link our thin film measurements to the published bulk results: Since only a few hundred nanometers of YIG close to the Pt contribute to the measured SSE signals at RT, it is not surprising that we obtain SSC signals for our thickest samples in the order of 1.5 $\mu\text{V/K}$, in line with bulk material measurements [26, 35], using a similar definition of the temperature difference.

In conclusion, we show that SSE features a characteristic increase and saturation of the signal with increasing YIG film thickness. As we observe thickness-dependent changes of the spin Seebeck signal even within series of samples with identical magnetic properties, we can rule out a dominating influence of magnetic properties or the magnetoresistance effect in the Pt detection layers. Instead we present a model that attributes this characteristic behavior to a finite propagation length of thermally excited magnons, created in the bulk of the ferromagnetic material. An increase and saturation of the SSC with increasing YIG film thickness has also been predicted by a theory of S. Hoffman et al. [36], who attribute a saturation of the SSE signal for large thicknesses also to the finite propagation length of thermally excited magnons. From the evaluation of our data at RT measured in samples grown by PLD, we obtain a mean propagation length of the order of 100 nm for thermally excited magnons, in agreement with other studies predicting a finite propagation length of thermally excited magnons of the order of 100 nm [37]. For LPE grown samples, we can observe a constant signal at RT in line with a propagation length below 1 μm . Measurements at 50 K reveal that the magnon propagation length is coupled to the absolute system temperature as we find a length of $\sim 7 \mu\text{m}$, in quan-

titative agreement with the results of our simulations, which estimate the propagation length of the order of 10 μm for low temperatures.

* Graduate School Materials Science in Mainz, Staudinger Weg 9, 55128, Germany

- [1] E. Saitoh, M. Ueda, H. Miyajima, and G. Tatara, *Appl. Phys. Lett.* **88**, 182509 (2006).
- [2] Y. Kajiwara, K. Harii, S. Takahashi, and J. Ohe, *Nature* **464**, 262 (2010).
- [3] K. Uchida, S. Takahashi, K. Harii, J. Ieda, W. Koshibae, K. Ando, S. Maekawa, and E. Saitoh, *Nature* **455**, 778 (2008).
- [4] C. M. Jaworski, J. Yang, S. Mack, D. D. Awschalom, J. P. Heremans, and R. C. Myers, *Nature Mat.* **9**, 898 (2010).
- [5] K. Uchida, J. Xiao, H. Adachi, J. Ohe, S. Takahashi, J. Ieda, T. Ota, Y. Kajiwara, H. Umezawa, H. Kawai, G. E. W. Bauer, S. Maekawa, and E. Saitoh, *Nature Mat.* **9**, 894 (2010).
- [6] H. Adachi, K. Uchida, E. Saitoh, J.-i. Ohe, S. Takahashi, and S. Maekawa, *Appl. Phys. Lett.* **97**, 252506 (2010).
- [7] M. Weiler, M. Althammer, F. Czeschka, H. Huebl, M. Wagner, M. Opel, I.-M. Imort, G. Reiss, A. Thomas, R. Gross, and S. Goennenwein, *Phys. Rev. Lett.* **108**, 106602 (2012).
- [8] J. Lustikova, Y. Shiomi, Z. Qiu, T. Kikkawa, R. Iguchi, K. Uchida, and E. Saitoh, *J. Appl. Phys.* **116**, 153902 (2014).
- [9] J. Xiao, G. E. W. Bauer, K. Uchida, E. Saitoh, and S. Maekawa, *Phys. Rev. B* **81**, 214418 (2010).
- [10] J. Ohe, H. Adachi, S. Takahashi, and S. Maekawa, *Phys. Rev. B* **83**, 115118 (2011).
- [11] S. Y. Huang, X. Fan, D. Qu, Y. P. Chen, W. G. Wang, J. Wu, T. Y. Chen, J. Q. Xiao, and C. L. Chien, *Phys. Rev. Lett.* **109**, 107204 (2012).
- [12] Y. M. Lu, Y. Choi, C. M. Ortega, X. M. Cheng, J. W. Cai, S. Y. Huang, L. Sun, and C. L. Chien, *Phys. Rev. Lett.* **110**, 147207 (2013).
- [13] D. Qu, S. Y. Huang, J. Hu, R. Wu, and C. L. Chien, *Phys. Rev. Lett.* **110**, 067206 (2013).
- [14] K. Uchida, M. Ishida, T. Kikkawa, A. Kirihara, T. Murakami, and E. Saitoh, *J. Phys.: Condens. Matter* **26**, 343202 (2014).
- [15] N. Roschewsky, M. Schreier, A. Kamra, F. Schade, K. Ganzhorn, S. Meyer, H. Huebl, S. Geprags, R. Gross, and S. T. B. Goennenwein, *Appl. Phys. Lett.* **104**, 202410 (2014).
- [16] M. Agrawal, V. I. Vasyuchka, A. A. Serga, A. Kirihara, P. Pirro, T. Langner, M. B. Jungfleisch, A. V. Chumak, E. T. Papaioannou, and B. Hillebrands, *Phys. Rev. B* **89**, 224414 (2014).
- [17] M. Agrawal, A. A. Serga, V. Lauer, E. T. Papaioannou, B. Hillebrands, and V. I. Vasyuchka, *Appl. Phys. Lett.* **105**, 092404 (2014).
- [18] M. A. Gilleo and S. Geller, *Phys. Rev.* **110**, 73 (1958).
- [19] S. Geller, G. P. Espinosa, and P. B. Crandall, *J. Appl. Cryst.* **2**, 86 (1969).
- [20] M. C. Onbasli, A. Kehlberger, D. H. Kim, G. Jakob, M. Klau, A. V. Chumak, B. Hillebrands, and C. A. Ross, *APL Materials* **2**, 106102 (2014).
- [21] L. Bi, J. Hu, P. Jiang, D. H. Kim, G. F. Dionne, L. C. Kimerling, and C. A. Ross, *Nature Photon.* **5**, 758 (2011).
- [22] See Supplemental Material at [URL] for further information about sample production and structural characterization [S1], magnetization and magnetoresistance properties [S2], SSE measurement method and setup [S3] and determination of the spin diffusion length of the Pt detection layer [S4].
- [23] V. Castel, N. Vlietstra, J. Ben Youssef, and B. J. van Wees, *Appl. Phys. Lett.* **101**, 132414 (2012).
- [24] M. Isasa, E. Villamor, L. E. Hueso, M. Gradhand, and F. Casanova, *Phys. Rev. B* **91**, 024402 (2015).
- [25] W. Kraus and G. Nolze, *J. Appl. Cryst.* **29**, 301 (1996).
- [26] K. Uchida, H. Adachi, T. Ota, H. Nakayama, S. Maekawa, and E. Saitoh, *Appl. Phys. Lett.* **97**, 172505 (2010).
- [27] A. Kehlberger, G. Jakob, M. C. Onbasli, D. H. Kim, C. A. Ross, and M. Klau, *J. Appl. Phys.* **115**, 17C731 (2014).
- [28] A. Kirihara, K. Uchida, Y. Kajiwara, M. Ishida, Y. Nakamura, T. Manako, E. Saitoh, and S. Yoroza, *Nature Mat.* **11**, 686 (2012).
- [29] M. B. Jungfleisch, V. Lauer, R. Neb, A. V. Chumak, and B. Hillebrands, *Appl. Phys. Lett.* **103**, 022411 (2013).
- [30] H. Nakayama, M. Althammer, Y.-T. Chen, K. Uchida, Y. Kajiwara, D. Kikuchi, T. Ohtani, S. Geprags, M. Opel, S. Takahashi, R. Gross, G. E. W. Bauer, S. T. B. Goennenwein, and E. Saitoh, *Phys. Rev. Lett.* **110**, 206601 (2013).
- [31] C. Du, H. Wang, F. Yang, and P. C. Hammel, *Phys. Rev. Applied* **1**, 044004 (2014).
- [32] U. Nowak, "Handbook of magnetism and advanced magnetic materials," (John Wiley & Sons, 2007) Chap. Classical Spin-Models.
- [33] U. Ritzmann, D. Hinzke, and U. Nowak, *Phys. Rev. B* **89**, 024409 (2014).
- [34] U. Ritzmann, D. Hinzke, A. Kehlberger, E. Guo, M. Klau, and U. Nowak, arXiv:1506.05290.
- [35] K. Uchida, T. Nonaka, T. Kikkawa, Y. Kajiwara, and E. Saitoh, *Phys. Rev. B* **87**, 104412 (2013).
- [36] S. Hoffman, K. Sato, and Y. Tserkovnyak, *Phys. Rev. B* **88**, 064408 (2013).
- [37] A. A. Kovalev and Y. Tserkovnyak, *Europhys. Lett.* **97**, 67002 (2012).

The authors would like to thank Sebastian Gonnenwein and Rudolf Gross from the Walther-Meissner-Institute for valuable discussions and the Deutsche Forschungsgemeinschaft (DFG) for financial support via SPP 1538 "Spin Caloric Transport", the Graduate School of Excellence Materials Science in Mainz (MAINZ) GSC 266 and the SFB 767 "Controlled Nanosystems: Interaction and Interfacing to the Macroscale" in Konstanz, the German Ministry for Education and Science "Mainz-MIT Seed Fund" (BMBF 01DM12012), the EU (IFOX, NMP3-LA-2012246102, INSPIN FP7-ICT-2013-X 612759, MASPIC, ERC-2007-StG 208162) the Solid-State Solar-Thermal Energy Conversion Center (S3TEC) supported by Dept. of Energy, DE-SC0001299 and the National Science

Foundation.